The Astrophysical Journal Supplement Series, 221:24 (14pp), 2015 December doi:10.1088/0067-0049/221/2/24


# THE SDSS-III APOGEE SPECTRAL LINE LIST FOR *H*-BAND SPECTROSCOPY

M. Shetrone[1], D. Bizyaev[2,3], J. E. Lawler[4], C. Allende Prieto[5,6], J. A. Johnson[7], V. V. Smith[8], K. Cunha[9,10], J. Holtzman[11], A. E. García Pérez[12], Sz. Mészáros[13], J. Sobeck[12], O. Zamora[5,6], D. A. García-Hernández[5,6], D. Souto[5,9], D. Chojnowski[2], L. Koesterke[14], S. Majewski[12], and G. Zasowski[15]
[1] University of Texas at Austin, McDonald Observatory, USA
[2] Apache Point Observatory and New Mexico State University, P.O. Box 59, Sunspot, NM, 88349-0059, USA
[3] Sternberg Astronomical Institute, Moscow State University, Moscow, Russia
[4] Department of Physics, University of Wisconsin-Madison, 1150 University Avenue, Madison, WI 53706, USA
[5] Instituto de Astrofísica de Canarias, Calle Vía Lactea s/n, E-38205 La Laguna, Tenerife, Spain
[6] Departamento de Astrofísica, Universidad de La Laguna, E-38206 La Laguna, Tenerife, Spain
[7] Department of Astronomy, The Ohio State University, Columbus, OH 43210, USA
[8] National Optical Astronomy Observatory, 950 North Cherry Avenue, Tucson, AZ 85719, USA
[9] Observatório Nacional, Rua General Jose Cristino, 77, 20921-400 São Cristóvão, Rio de Janeiro, RJ, Brazil
[10] University of Arizona, Tucson, AZ 85719, USA
[11] Department of Astronomy, New Mexico State University, Las Cruces, NM 88003, USA
[12] Department of Astronomy, University of Virginia, P.O. Box 400325, Charlottesville, VA 22904-4325, USA
[13] ELTE Gothard Astrophysical Observatory, H-9704 Szombathely, Szent Imre herceg st. 112, Hungary
[14] The University of Texas at Austin, Texas Advanced Computing Center, USA
[15] Department of Physics and Astronomy, Johns Hopkins University, Baltimore, MD 21218, USA
*Received 2015 February 12; accepted 2015 October 6; published 2015 November 25*

## ABSTRACT

We present the *H*-band spectral line lists adopted by the Apache Point Observatory Galactic Evolution Experiment (APOGEE). The APOGEE line lists comprise astrophysical, theoretical, and laboratory sources from the literature, as well as newly evaluated astrophysical oscillator strengths and damping parameters. We discuss the construction of the APOGEE line list, which is one of the critical inputs for the APOGEE Stellar Parameters and Chemical Abundances Pipeline, and present three different versions that have been used at various stages of the project. The methodology for the newly calculated astrophysical line lists is reviewed. The largest of these three line lists contains 134,457 molecular and atomic transitions. In addition to the format adopted to store the data, the line lists are available in MOOG, Synspec, and Turbospectrum formats. The limitations of the line lists along with guidance for its use on different spectral types are discussed. We also present a list of *H*-band spectral features that are either poorly represented or completely missing in our line list. This list is based on the average of a large number of spectral fit residuals for APOGEE observations spanning a wide range of stellar parameters.

*Key words:* atomic data – line: identification – methods: laboratory: atomic – molecular data

*Supporting material:* machine-readable tables, tar.gz files

## 1. INTRODUCTION

The Apache Point Observatory Galactic Evolution Experiment (APOGEE) is one of the programs that was carried out on the Sloan Foundation 2.5-m Telescope (Gunn et al. 2006) by the third stage of the Sloan Digital Sky Survey (SDSS-III; Eisenstein et al. 2011). APOGEE obtained high-resolution ($R \sim 22{,}500$) and high signal-to-noise ratio ($S/N > 100$) spectra in the *H* band (1.51–1.70 $\mu$m) for more than 100,000 cool giant stars (see Zasowski et al. 2013, for more information about targeting) spanning all components of the Milky Way (Majewski et al. 2015). Stellar parameters and individual chemical abundances are derived from the combined APOGEE spectra (Nidever et al. 2015) with the APOGEE Stellar Parameters and Chemical Abundances Pipeline (ASPCAP), which is described in detail in García Pérez et al. (2015). ASPCAP uses a grid of synthetic spectra to determine stellar parameters and abundances by finding the best match to the observed spectra interpolating within the grid. For the public data releases, the synthetic spectra have been calculated using the spectral synthesis code ASS$\epsilon$T (Koesterke 2009), which itself is based, in part, on the synthesis code Synspec (Hubeny & Lanz 2011).

In order to run ASPCAP on the first year of APOGEE results (DR10; Ahn et al. 2014), an initial line list was generated and adopted. In subsequent years, improvements were made and different methodologies were adopted in the line list used for the release of the full three year data set of APOGEE (DR12; Alam et al. 2015). The APOGEE internal naming scheme for the DR10 and DR12 line lists are 20110510 and 20131216, respectively. In the years between DR10 and DR12, García Pérez et al. (2013), Smith et al. (2013) and Cunha et al. (2015) made use of an intermediate line list, 20120216. The APOGEE naming scheme includes the year, month and day label to keep track of changes made to each line list. Because these dated names are long and difficult to associate with each data product we will refer hereafter to 20110510, 20120216, and 20131216 as DR10, INT, and DR12 line lists, respectively. The line list continues to evolve in APOGEE-2, an extension of the project as part of SDSS-IV.

In this paper we document the methodologies employed by APOGEE to produce the three *H*-band line lists that were used by ASPCAP (and several independent analyses) to derive stellar parameters and chemical abundances. The first section of this paper describes the base line list taken from literature sources, including those derived from laboratory, theoretical, and astrophysical sources. Parameters of the transitions, even if they are well studied, have associated uncertainties. We aspire to improve on the theoretical line parameters by comparing

synthetic spectra with the observed high-resolution spectra of two well known stars (the Sun and Arcturus) to produce "astrophysical" oscillator strength values and damping constants. In the second section, we describe the code used to derive our astrophysical log(*gf*) and damping parameters. We also describe some issues identified in the INT and DR12 APOGEE line lists and describe the impact these issues have on the stellar parameters and abundances derived from those lists. In Section 4 we detail the stellar features which appear to be missing from our line list, based on synthesis from a large portion of the DR12 stellar library. In the last section, we describe the line list formats and review the performance of the line list as described in a number of papers in the literature.

## 2. BASE LINE LIST FROM LITERATURE

### 2.1. Oscillator Strengths

This section describes the various literature sources that were considered for the base line list. Criteria for accepting and rejecting various sources are presented. When we refer to the oscillator strengths, we use the standard expression log(*gf*) for the base ten logarithm of the product of the lower level degeneracy and absorption oscillator strength.

#### 2.1.1. Molecules

The molecular line lists are taken almost entirely from literature sources. For DR10 an attempt was made to fit the molecular features to the very weak lines seen in the Sun in order to define solar gf values. For the INT and DR12 line lists, the molecular astrophysical log(*gf*) changes were removed in favor of adopting the best literature values available. Below we discuss separately each molecule and note references adopted, as well as other line lists that were tested.

##### 2.1.1.1. CN

We used the Kurucz (CD-ROM 18) CNAX.ASC and CNBX.ASC lists as the base line list. This combined list was tested against the line list in Melendez & Barbuy (1999, MB99). The latter is a hybrid of theoretical log(*gf*) values provided by S. P. Davis and astrophysical values fit to the Sun using abundances from Grevesse et al. (1996). Our tests indicated that the line positions and strengths from MB99 were found to provide overall a better match to the CN features in the Sun and Arcturus. Thus, the MB99 list was adopted, while we kept in our line list any of the CN lines which were in the Kurucz line list and not in MB99. We tested this composite list against the 2010 version of the Plez CN line list (private communication) and found that our composite list better fit the Sun and Arcturus spectra, i.e., resulting in fewer poorly fit lines and fewer predicted lines without associated observable features. For DR10 we changed the CN molecules' log(*gf*) values by +0.03 to fit the strongest lines in the Sun based on a visual inspection. For INT and DR12 we removed the astrophysical log(*gf*) offset and the composite line list (MB99 + Kurucz) was adopted in the final line list.

##### 2.1.1.2. CO

We tested the Kurucz (CD-ROM 18) COAX.ASC and COXX.ASC composite line list against the line list from Goorvitch (1994) and found the latter to be slightly better in strength, but not in wavelength. Thus we adopt the Goorvitch log(*gf*) values for the CO lines in the Kurucz list, while keeping the original wavelengths as in the Kurucz line list. There were no lines in the Goorvitch list that were not in the Kurucz list. We retained all lines in the Kurucz list that were not included in the Goorvitch list. For DR10 we changed the CO molecules log(*gf*) values by −0.10 to fit the strongest lines in the Sun based on an overall visual inspection of the obtained fits. For INT and DR12 we removed any astrophysical log(*gf*) values and the Goorvitch and Kurucz hybrid line list was adopted.

##### 2.1.1.3. OH

We tested the Kurucz (CD-ROM 18) OH.ASC list against that of Goldman et al. (1998) and found the Goldman lines to provide a better fit to the Sun and Arcturus. We adopted the OH lines from Goldman et al. (1998) for our base line list. For DR10 we changed the OH molecules log(*gf*) values by −0.07 to fit the strongest lines in the Sun based on an overall visual inspection of the obtained fits. For INT and DR12 we removed any astrophysical log(*gf*) values, and the Goldman+Kurucz OH lines were adopted as the final product.

##### 2.1.1.4. $H_2$

The Kurucz (CD-ROM 18) H2.ASC was adopted as a base line list but was supplemented by a few additional lines from hdxx.asc (Kurucz web site, http://kurucz.harvard.edu/molecules/). For DR12 we reduced the log(*gf*) value for the $H_2$ line at 16586.664 Å by 6.0 dex, based on a poor fit to the Arcturus spectrum and to be in line with the other log(*gf*) values for the $H_2$ lines.

##### 2.1.1.5. $C_2$

The Kurucz (CD-ROM 18) C2AX.ASC, C2BA.ASC, C2DA.ASC, and C2EA.ASC files were used as a base line list. For DR12 we fixed some $C_2$ AX features that were clearly discrepant in Arcturus by replacing their log(*gf*) values with those from Brault et al. (1982) and Kokkin et al. (2007).

##### 2.1.1.6. SiH

We used the Kurucz (CD-ROM 18) HYDRIDES.ASC list for the SiH features as a base line list. While these features should be visible in only very few giant and dwarf stars, they have been included in the line list for completeness.

##### 2.1.1.7. FeH

For DR12, several FeH line lists were tested, including lines from Langhoff & Bauschlicher (1990) as implemented in the Uppsala spectral synthesis code BSYN, and Dulick et al. (2003) as implemented by Kurucz in fehfx.asc (Kurucz web site, http://kurucz.harvard.edu/molecules/). We tested these on *H*-band NIRSPEC spectra of the cool dwarf stars GL436 (Prato et al. 2002) and GL763 (Bender et al. 2005), kindly provided by C. Bender. Based on the synthetic spectra generated using these two line lists and stellar parameters, we expected to find a large number of weak FeH features. We searched for conspicuous spectral features in the observed spectra at locations that both line lists predicted there to be relatively isolated FeH lines, but did not find any consistently accurate predictions. In addition, we tried to determine if FeH lines would help in a statistical sense even if the strongest features could not be identified. The first test was a cross-

correlation of a synthetic spectrum of pure FeH against the observed spectra; no peak was found at the rest velocity of either star. The second test was to subtract the synthetic spectra with and without the FeH features from the observed spectrum; in both cases the scatter increased with the inclusion of the FeH lines. From these tests we conclude that the current FeH line lists would not assist in our analysis of the APOGEE spectra, thus the FeH lines were not included for DR12.

#### 2.1.2. Atoms

For the atomic features, we compiled an atomic line list from a variety of different sources. As a base line list, we started with the Kurucz line list gfhy3000.dat (Kurucz web site, http://kurucz.harvard.edu/linelists/gfhyper100/). In this line list we included, in separate columns, lab data, the "best" empirical log(*gf*) values in the literature, and our astrophysical log(*gf*) values. This line list contains many more lines than are typically detectable in *H*-band stellar spectra of cool giants, but all lines were retained in the line list as it may aid future investigations of extremely hot stars, investigations of nebular features, or laboratory efforts.

##### 2.1.2.1. Laboratory Data

The gold standard for line list data is high-quality laboratory measurements of energy levels, branching fractions, and lifetimes. With this type of data, we will have not only the best quality values but also quantifiable errors that can be used to constrain empirical changes from laboratory values, as will be discussed in Section 3. In this section we consider both true laboratory measurements and any theoretical measurements that have such well constrained theoretical uncertainty as to allow uncertainties to be included. For example, in the case of hydrogen (Paschen lines), the National Institute of Standards and Technology database (NIST; Kramida et al. 2014) gives the uncertainties in the log(*gf*) as AAA or $\leqslant$0.3%. Within this paper we will refer to any log(*gf*) that has quantifiable errors as laboratory data. Table 1 contains the origins of the different lab sources adopted in our list. Most of these were compiled in the NIST database and we adopt their usual grade-to-uncertainty conversion (Table 2). In the case of Ti I, we adopted log(*gf*) values from Lawler et al. (2013) over Blackwell-Whitehead et al. (2006) when available.

In addition to the laboratory log(*gf*) values from the sources above, for the DR12 line list we updated the theoretical wavelengths with wavelengths from the following sources.

1. Ti I wavelengths from Saloman (2012).
2. Ti II wavelengths from Saloman (2012).
3. V I wavelengths from Thorne et al. (2011).
4. Cr I wavelengths from Saloman (2012).
5. Cr II wavelengths from Saloman (2012).
6. Rb I wavelengths from Sansonetti (2006).

**Table 1**
Laboratory Sources for Oscillator Strengths

| Species | Source |
|---|---|
| H I | NIST—Wiese & Fuhr (2009) |
| He I | NIST—Wiese & Fuhr (2009) |
| C I | NIST—Wiese et al. (1996), NIST—Wiese & Fuhr (2007) |
| C II | NIST—Wiese et al. (1996), NIST—Wiese & Fuhr (2007) |
| C III | NIST—Wiese et al. (1996) |
| C IV | NIST—Wiese et al. (1996) |
| N I | NIST—Wiese et al. (1996), NIST—Wiese & Fuhr (2007) |
| N II | NIST—Wiese et al. (1996), NIST—Wiese & Fuhr (2007) |
| N III | NIST—Wiese et al. (1996) |
| N V | NIST—Wiese et al. (1996) |
| O I | NIST—Wiese et al. (1996) |
| O II | NIST—Wiese et al. (1996) |
| O III | NIST—Wiese et al. (1996) |
| Na I | NIST—Kelleher & Podobedova (2008), NIST—Sansonetti (2008) |
| Mg I | NIST—Kelleher & Podobedova (2008) |
| Mg II | NIST—Kelleher & Podobedova (2008) |
| Al I | NIST—Kelleher & Podobedova (2008) |
| Si I | NIST—Kelleher & Podobedova (2008) |
| Si II | NIST—Kelleher & Podobedova (2008) |
| Si III | NIST—Kelleher & Podobedova (2008) |
| S I | NIST—Podobedova et al. (2009) |
| Ar I | NIST—Wiese et al. (1969) |
| K I | NIST—Sansonetti (2008), NIST—Wiese et al. (1969) |
| Ti I | Lawler et al. (2013), NIST—Blackwell-Whitehead et al. (2006) |
| Ti II | Wood et al. (2013) |
| V I | NIST—Sansonetti (2008), NIST—Wiese et al. (1969) |
| Fe I | Ruffoni et al. (2013) |

**Note.**
The species with NIST indicated as a Source contain the noted references in the NIST database.

**Table 2**
Adopted Uncertainties for the Oscillator Strengths

| Grade | Uncertainty |
|---|---|
| AAA | $\leqslant$0.3% |
| AA | $\leqslant$1% |
| A+ | $\leqslant$2% |
| A | $\leqslant$3% |
| B+ | $\leqslant$7% |
| B | $\leqslant$10% |
| C+ | $\leqslant$18% |
| C | $\leqslant$25% |
| D+ | $\leqslant$40% |
| D | $\leqslant$50% |
| E | >50% |

**Note.**
Grade-to-uncertainty conversion for the oscillator strengths as defined by NIST.

##### 2.1.2.2. Literature Astrophysical and Theoretical log(*gf*) Values

The goal of these efforts is for the line list to be a comprehensive list of all *H*-band transitions which may appear in APOGEE spectra. With this goal in mind, we have taken the base line list (as defined in 2.1.2) and augmented it with additional lines from various theoretical predictions. Since we are not the first to generate *H*-band line lists, we also tested some of these literature compilations against our base list to determine if we might improve the list with transitions from these sources. Since there are few *H*-band transitions known for elements heavier than copper, we placed extra emphasis and effort on $Z > 30$ transitions.

A careful review of all pages of the Kurucz web site (http://kurucz.harvard.edu/atoms.html) revealed a few additional Ti, Fe, and Cr transitions, which were added to the base line list. We tested the MB99, Ryde et al. (2009), and Ryde et al. (2010) line lists and found their log(*gf*) values to provide a better fit to the Sun than the base line list. This should not be surprising as

these three references are based on astrophysical solar log($gf$) values. All of these log($gf$) values were added, giving preference to the most recent line lists, e.g., Ryde et al. (2009) over MB99, for any features in common between the lists. We added Ce III lines from Wyart & Palmeri (1998) and Y II lines from the DREAM compilation (Biémont et al. 1999, Feb. 2011 download). We replaced all log($gf$) values for Ca I and Ca II with the values given in Hansen et al. (1999) and Laughlin (1992), respectively.

#### 2.1.2.3. Hyper-fine Splitting

For DR12 we adopted the energy levels for V I lines from Thorne et al. (2011), and we added the V hyper-fine splitting (HFS) components using the coefficients of Palmeri et al. (1997), Palmeri et al. (1995), and Güzelçimen et al. (2011). Güzelçimen et al. (2014) and Wood et al. (2014) have published laboratory measurements for the V energy levels since the DR12 line list was generated. These values produce HFS components that are in excellent agreement with the earlier theoretical predictions. Based on the Na I components from Safronova et al. (1999) and Happer (1974), the HFS is too small to impact the line profile or abundance analysis.

For Al the HFS can be significant and its exclusion from the APOGEE line lists deserves comment. Using the HFS components from Falkenburg & Zimmermann (1979) and Sur et al. (2005) we find that for the weaker Al lines the impact of HFS is less than 0.1 dex (a typical uncertainty for APOGEE) while for the strongest line at 16755 it has offsets as large as 0.4 dex for the coolest, most metal-rich giants. ASPCAP measures abundances from all of the Al features and thus will potentially have a bias toward abundances which are slightly too high and a function of line strength (largely metallicity and effective temperature). Examination of the slope and scatter of the Al abundances for open clusters in the APOGEE calibration sample (Figure 5 in Holtzman et al. 2015) suggests that this bias is less than 0.1 dex. A secondary check can be made by comparing literature determinations of Al in globular clusters compared to those using an APOGEE line list as in Mészáros et al. (2015), Figure 4. If HFS was a significant influence in these stars then one would expect that the [Al/Fe] enhanced abundances would be biased positively compared to the [Al/Fe] "normal" stars and that the affect would be strongest in the most metal-rich clusters. There is a small trend among the clusters of the order of 0.2 dex. While Al HFS will be added in future versions of the APOGEE line list, users of this line list in the future should be aware of this limitation and perhaps avoid the use of the strongest Al feature as was done in Smith et al. (2013).

### 2.2. Damping

The line width for a spectral feature is a complicated function of stellar rotation, thermal broadening, turbulence, and surface convection, and several other types of quantum mechanical broadening that mostly impact strong lines, including Stark, resonance, and van der Waals. Broadening coefficients are often included in line lists, and one of the most important of these is the van der Waals broadening. In this work, what we refer to as "damping" is actually the log of the broadening coefficient: van der Waals collisional damping divided by the number density of hydrogen, or $\log(\Gamma_6/N_{\rm H}) = 17v^{3/5}C_6^{2/5}$, where $v$ is the velocity (set by thermal motions with $T_{\rm eff} = 10{,}000$) and $C_6$ is the interaction constant. There are only a few different sources for the damping or $C_6$ values in the $H$ band: the Kurucz compilation, MB99, Ryde et al. (2009, 2010). MB99 actually used several different methods to get the damping: fits to the solar spectrum, values out of Barklem et al. (1998) and other references.

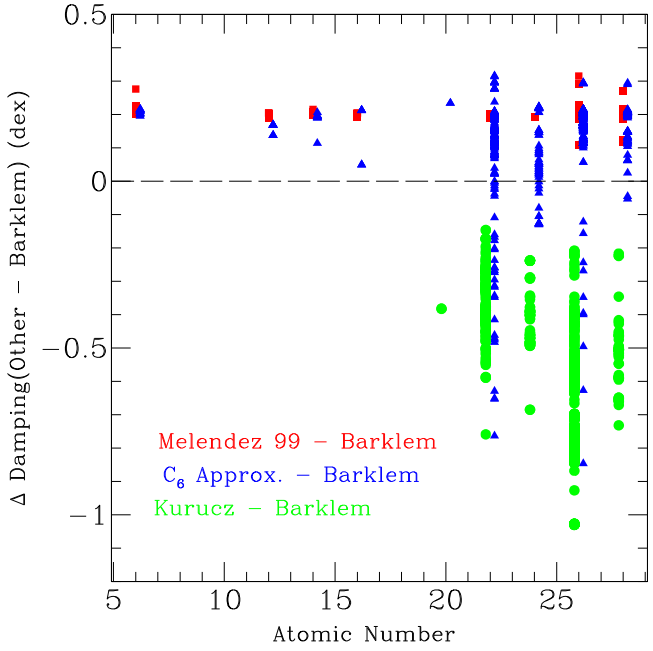


**Figure 1.** Difference between the log damping values from various sources and the Barklem values. The $x$ axis shows atomic number. The red squares are MB99—Barklem, the blue triangles are $C_6$ approximation—Barklem, and the green circles are Kurucz—Barklem. The point type has been offset slightly to avoid them overlapping each other. The dashed line at $\Delta = 0$ is provided to guide the eye.

The Barklem web site (http://www.astro.uu.se/~barklem/, v2.0 Barklem et al. 1998) has codes for calculating the van der Waals damping. However, these codes only work for certain values of the effective principal quantum number. We downloaded v2 and ran it for all of the transitions within range. For many of the IR transitions the effective principal quantum number is outside of the Barklem grid.

It is possible to approximate the $C_6$ values as $6.46E{-}34\ \Delta r^2$, where $\Delta r$ is the unit-less difference in the mean square radius of the two energy levels (Unsöld 1955). The radius can be described roughly as $r = 0.5 * n^2 * (5 * n^2 + 1 - 3 * l(l+1))$ (MB99) where $n = 1/(\Delta{\rm EP}/\chi)^{0.5}$, $\Delta$EP is the difference between the energy level of the transition and the ionization energy ($\chi$), and $l$ is the orbital angular momentum quantum number. This approximation yields a $C_6$ value 10 times larger than that calculated by Unsöld (1955).

We assumed the Barklem values to be the best possible source for theoretically derived damping constants. In Section 3.3 we show that these theoretical values are very close to the calculated values based on comparisons to the solar spectrum. Figure 1 shows the difference between the different damping constants and the Barklem values as a function of atomic mass number for those lines in common. The Kurucz damping constants are systematically too small by several tenths of a dex, while the $C_6$ approximation and MB99 values are too large by a few tenths of a dex. From this assessment,

our ranked preferences for adopted damping values for the base line list are:

1. Barklem et al. (1998) whenever possible;
2. Ryde et al. (2009) and Ryde et al. (2010);
3. MB99;
4. the $C_6$ approximation given in this section;
5. Kurucz values.

## 3. SEMI-AUTOMATED "ASTROPHYSICAL" LINE LIST CALCULATIONS

It is possible to improve upon theoretical log(*gf*) and damping values by comparing line profiles and strengths of well understood spectra to synthetic spectra. Even laboratory measurements with significant error bars could be improved by this type of comparison if done within the errors of the measurement. We refer to these corrections based on observed spectra as "astrophysical" line parameters. In this section we describe the software and methodology we created to generate astrophysical line parameters and compare those parameters to the base line list values. It should be noted that in making changes to the atomic line parameters to match the observations one is also masking systematic errors in the model atmospheres and the line formation calculations.

### 3.1. Astrophysical Software and Methodology

We have developed a code that can vary the log(*gf*) and damping values in a line list to match one or more observed spectra. The final product of the code is a set of astrophysical log(*gf*) and damping values that we adopt in the final line list. This code relies on having accurate stellar parameters for the observed stellar spectra and a constrained and accurate base line list.

The code was developed within the APOGEE team by DB and is available through the Astrophysics Source Code Library (Bizyaev & Shetrone 2015). This code has evolved, and the version used for DR12 is more complex than that used for DR10. Below we document the state of the code as implemented for DR12 and describe the significant changes that were made after DR10.

The code is written in IDL as a wrapper around the spectral synthesis code MOOG (Sneden 1974). For DR10 the 2009 version of MOOG was used, and for DR12 the 2013 version was used. Zamora et al. (2015) conducted an analysis of the differences between synthetic spectra computed with both MOOG and ASS$\epsilon$T and found the differences to be very minor for the Sun and Arcturus, $<0.01$ except around the hydrogen lines. The astrophysical gf-fitting code starts with an input line list, which in our case is the best laboratory and literature values available between 1.5 and 1.7 $\mu$m (see Section 2). For spectral comparison we adopt an *H*-band center-of-disk (COD) atlas for the Sun (Livingston & Wallace 1991) and an Arcturus flux atlas (Hinkle et al. 1995). The adopted solar and Arcturus stellar parameters and abundances are listed in Tables 3 and 4. The DR10 solar model was created from a grid of Kurucz Atlas models (Castelli et al. 1997) with computed Opacity Distribution Functions (ODFs). We interpolate within this grid using the code "makekuruczpublic" (McWilliam et al. 1995). Unfortunately, after the DR10 calculations were made, a mistake entered into our methodology and the synthesis of the Sun was done as if it were a full flux spectrum, rather than a COD calculation. This is noted in Table 3 as "not COD." In Section 3.2.1 we discuss the impact of this on the INT and DR12 line lists and how it may impact the subsequently derived abundances.

**Table 3**
Model Atmospheres Adopted for Astrophysical log(*gf*) Value Calculations

| Model | $T_{\rm eff}$ | log(g) | [Fe/H] | $v_t$ | Notes |
|---|---|---|---|---|---|
| | | | Sun | | |
| DR10 | 5780 | 4.40 | +0.00 | 1.10 | Kurucz ODFNEW |
| INT | 5777 | 4.44 | +0.00 | 1.10 | Kurucz ODFNEW; not COD |
| DR12 | 5777 | 4.44 | +0.00 | 1.10 | Kurucz ODFNEW; not COD |
| | | | Arcturus | | |
| DR10 | 4290 | 1.55 | −0.55 | 1.67 | MARCS |
| INT | 4286 | 1.66 | −0.52 | 1.70 | Kurucz NOVER |
| DR12 | 4286 | 1.66 | −0.52 | 1.70 | new revised Kurucz |

**Note.** Not COD: these syntheses were mistakenly calculated as full flux calculations within MOOG and not set as center of disk (COD).

**Table 4**
Abundances Adopted for Astrophysical log(*gf*) Value Calculation

| Atomic | | Sun | | | Arcturus | | |
|---|---|---|---|---|---|---|---|
| Number | Species | DR10 | INT | DR12 | DR10 | INT | DR12 |
| 6 | C | 8.43 | 8.43 | 8.39 | 7.88 | 8.27 | 7.96 |
| 7 | N | 7.83 | 7.83 | 7.78 | 7.21 | 7.26 | 7.64 |
| 8 | O | 8.69 | 8.69 | 8.66 | 7.59 | 8.54 | 8.64 |
| 11 | Na | 6.27 | 6.27 | 6.17 | 5.73 | 5.65 | 5.65 |
| 12 | Mg | 7.53 | 7.53 | 7.53 | 7.24 | 7.41 | 7.41 |
| 13 | Al | 6.43 | 6.43 | 6.37 | 6.24 | 6.15 | 6.15 |
| 14 | Si | 7.51 | 7.51 | 7.51 | 7.02 | 7.39 | 7.39 |
| 16 | S | 7.15 | 7.15 | 7.14 | 6.70 | 7.02 | 7.02 |
| 19 | K | 5.08 | 5.08 | 5.08 | 4.82 | 4.56 | 4.56 |
| 20 | Ca | 6.29 | 6.29 | 6.31 | 5.85 | 5.89 | 5.89 |
| 22 | Ti | 4.91 | 4.91 | 4.90 | 4.69 | 4.78 | 4.78 |
| 23 | V | 3.96 | 3.96 | 4.00 | 3.41 | 3.48 | 3.48 |
| 24 | Cr | 5.64 | 5.64 | 5.64 | 5.09 | 5.12 | 5.12 |
| 25 | Mn | 5.48 | 5.48 | 5.39 | 4.69 | 4.87 | 4.87 |
| 26 | Fe | 7.45 | 7.45 | 7.45 | 6.90 | 6.93 | 6.93 |
| 27 | Co | 4.87 | 4.87 | 4.92 | 4.32 | 4.40 | 4.40 |
| 28 | Ni | 6.20 | 6.20 | 6.23 | 5.65 | 5.71 | 5.71 |

The DR10 Arcturus model atmosphere was interpolated from the 2005 MARCS grid (Gustafsson et al. 2003, 2008, further expanded by B. Edvardsson 2015, private communication). The MARCS models have opacity sampling instead of ODFs; however, the MARCS models are spherical, with appropriate $\alpha$-enhancement at the metallicity of Arcturus, and thus were deemed to be more appropriate for DR10. Although the differences between the most recent Kurucz and MARCS models are minimal at the effective temperature and gravity of Arcturus (Zamora et al. 2015), we adopted a Kurucz model for Arcturus after DR10 to be consistent with the rest of the ASPCAP models. For the INT line list, we use the same Kurucz grid from which we pulled the solar model. We should note that the exact details of the Arcturus model atmosphere for DR10 and INT will have little impact on the final line list because, as will be described in more detail below, the final solar log(*gf*) fitting removed all but the weakest or most temperature/gravity sensitive features in the Arcturus log(*gf*) fitting. For DR12 the log(*gf*) fitting methodology changed so

the model was far more critical. For DR12 we adopted a model generated in the same way as the model atmosphere grid points were generated for ASPCAP, namely from the Kurucz Atlas 9 code (see Mészáros et al. 2012).

The solar abundances for DR10 and INT were adopted from Asplund et al. (2009), while for DR12 we adopted the abundances from Asplund et al. (2005). This change was made to make the assumed abundances in the line list consistent with those adopted in the Kurucz model atmospheres calculated for APOGEE (Mészáros et al. 2012; Zamora et al. 2015).

The Arcturus abundances were set with a number of considerations. Since we were concerned about misfitting the atomic features near molecular features, we forced the C, N, and O abundances to match those of Smith et al. (2013), who derived those abundances in an independent analysis in the *H*-band using line list INT. The C, N, and O abundances from Smith et al. (2013) are very similar (within ~0.05–0.10 dex) to those derived recently by Abia et al. (2012), who used NIR lines of CO, OH, and CN, as well as Sneden et al. (2014), who used optical $C_2$, [O I], and CN transitions. The mean and standard deviations of these 3 studies are A(C) = 8.01 ± 0.05, A(N) = 7.66 ± 0.02, and A(O) = 8.64 ± 0.03, with $^{12}C/^{13}C = 7.4 \pm 1.4$; the Arcturus C, N, and O abundances are therefore well-constrained in these recent independent studies. We wanted the abundances to be largely self-consistent with those adopted in the model atmosphere, so the abundances of Mg, Si, S, and Ti were all given $\alpha$-enhanced values of +0.4 above scaled solar, whereas all of the odd Z elements (except Al) and iron peak elements were given scaled solar values. Al has several very strong features with several other important features in its wings, thus we adopted a value to fit all three strong lines. This adopted value was close to that of Smith et al. (2013), who excluded the strongest line from their analysis. The abundance of Ca clearly deviates significantly from the other alpha elements, so we adopted a value close to that of Smith et al. (2013). For DR10 the Arcturus log(*gf*) values were only adopted for a small subset of those lines-of-interest (LOI) which were above the threshold in Arcturus but not in the Sun. For DR12 the adopted Arcturus abundances play a far more significant role because the final Arcturus and solar log(*gf*) values were averaged together, although the solar values were given more weight. In retrospect, the self-consistency requirement, i.e., forcing the abundances to match the model, should not have been a significant driver and may have resulted in a less optimal line list that resulted in an abundance inconsistency for Arcturus in ASPCAP (see Section 5.5.1 in Holtzman et al. 2015).

In order to match the line broadening in the Arcturus atlas spectrum, we convolved all synthetic spectra with an instrumental profile and a rotational profile ($v\sin i = 2.0\,\mathrm{km\,s^{-1}}$; Gray 1981; Gray & Brown 2006). The limb darkening for Arcturus in the NIR is assumed to be 0.46 (Claret 2000). Solar synthetic spectra were compared with the COD atlas spectrum, and therefore were not corrected for rotation but they were convolved with an instrumental profile. The instrument profile was determined from an analysis using cross-correlation against a synthetic spectrum generated from the base line list but avoiding the strongest lines.

For DR10 and INT we selected the LOI using the line strength (opacity at line center) tabulation built into MOOG which allowed us to remove extremely weak lines. For DR12 we refined this by running each line individually and noting the line depth. The number of strong lines in a spectrum varies significantly with stellar spectral type and with an adopted cutoff for the minimum line strength. We calculated the maximum line depth with respect to the normalized continuum for each line in the initial line list. Table 5 shows the number of atomic and molecular features deeper than the listed depth in the solar and Arcturus spectra. Since the target S/N for APOGEE program stars is 100, we considered evaluating only those lines that were deeper than 0.001 with respect to the normalized continuum. For reference the weakest lines visible in Figure 3 have a depth of 0.004 and equivalent widths of <0.6 mÅ and are well below the detection threshold in APOGEE spectra. The final set of LOI is the joint list for the Sun and Arcturus corresponding to the >0.001 level (see Table 5). Future improvements to the line fitting code will likely involve the entire line strength and not the depth at the line center as this would remove line depth variations due to damping and HFS differences from line to line.

**Table 5**
Number of Strong Lines in the Solar and Arcturus Spectra

| Limiting | Sun | | Arcturus | |
|---|---|---|---|---|
| Depth | All Lines | Atomic only | All Lines | Atomic Only |
| 1E-4 | 10775 | 3409 | 31192 | 4287 |
| 5E-4 | 5600 | 2426 | 19731 | 2819 |
| 1E-3 | 4291 | 2166 | 15919 | 2559 |
| 1E-2 | 1348 | 989 | 8758 | 1590 |

**Note.** The number of strong lines (atomic and molecular, or atomic only) in the synthetic spectra of the Sun and Arcturus in the range between 1.50 and 1.70 $\mu$m in dependence of the limiting line depth.

Once we had the LOI, we started evaluating them one by one in order of line strength, with the strongest line first. For each line we fit the spectral range within 0.8 Å around the line center. To account for possible wings of nearby strong lines, we calculated the contribution of all lines within 18 Å around each considered LOI. We evaluated two free parameters: radial velocity changes within $\pm 0.25\,\mathrm{km\,s^{-1}}$ (which also accounts for the uncertainty in the central wavelength) and log(*gf*), which is allowed to vary within the following set of rules:

1. for DR10 and INT, the lines with measured laboratory values were allowed to vary within 1 sigma of those laboratory measurements, and all other LOI were allowed to vary by −2 to +0.75 dex, and
2. for DR12, the lines with measured laboratory values were allowed to vary within 2 sigma of those laboratory measurements, and all other LOI were allowed to vary by −2 to +0.75 dex.

The reasoning behind the asymmetric limits on the log(*gf*) variation is motivated by the fact that there are bad and missing lines in the base line list. There are a number of strong theoretical lines without observed counterparts, and we want these lines to be strongly suppressed, which sets the lower limit of −2 dex in log(*gf*). There are also a number of observed lines without theoretical or laboratory counterparts in the base line list, and we do not want to inflate inappropriate very weak lines, which sets the upper limit of +0.75 dex in the log(*gf*). The line list was updated with new log(*gf*) values on the fly during the fitting. Spectral pieces around each LOI were fitted

using the downhill simplex optimization algorithm by Nelder & Mead (1965). Because the LOIs often overlapped, we performed the evaluation iteratively.

The treatment of HFS changed between the INT line list and the DR12 line list. Before DR12, no consideration was made to force the different components of an adjusted line to scale with each other. Thus, if the code required the strongest component of a line with HFS to be adjusted, then no change was made for weaker components. For DR12, we changed HFS component log(*gf*) values by the same amount.

For DR10 and INT the majority of the LOI were fit only to the Sun, but those lines that were not visible in the Sun (i.e., were below the depth threshold) but were visible in Arcturus were fit to Arcturus. LOI that were above the detection threshold in the Sun were fit again and superseded any corrections that were based on the Arcturus spectrum. Thus, LOI were either fit to Arcturus or the Sun. Atomic lines weaker than the cutoff, i.e., not a LOI, in both the Sun and Arcturus were left unchanged from the input line list's values. So for DR10 and INT, the following methodology was adopted.

1. Fit the LOI in the Sun for two iterations for the log(*gf*) values.
2. Fit the LOI in Arcturus for a single iteration for the log(*gf*) values.
3. Fit the LOI in the Sun for two iterations for the log(*gf*) values.
4. Fit the strongest LOI in the Sun for damping parameters.
5. Fit the LOI in the Sun for three final iterations of the log(*gf*) values.

For DR12 we implemented the use of both the solar and Arcturus spectra to constrain the astrophysical log(*gf*) values. To accomplish this we determined the astrophysical values from Arcturus and from the Sun independently instead of serially (as was done for DR10 and INT) and then weighted the solutions, with the Sun getting twice the weight as Arcturus because the abundances in the solar photosphere are also confirmed by the meteoritic values. Other weighting schemes are possible and will be considered for future line lists.

We noticed that most values of log(*gf*) settled down quickly after the second iteration over all LOI. We also evaluated the damping constant for the strongest lines, applying the same algorithm as for the derivation of the log(*gf*) values but using only the solar spectrum for the comparison. Our standard sequence of the line parameter adjustment process was $2 \times E\log(gf)$, $2 \times E\mathrm{damp}$, $n \times E\log(gf)$, where $E\log(gf)$ and $E\mathrm{damp}$ designate one iteration over the whole LOI list for log(*gf*) and for the damping constants, respectively.

We justified the number of necessary iterations by running a few long sequences "$2 \times E\log(gf)$, $2 \times E\mathrm{damp}$, $n \times E\log(gf)$" with n over 30. It was noticed that the log(*gf*) values for most of the LOIs settled down after the "$2 \times E\log(gf)$, $2 \times E\mathrm{damp}$, $2 \times E\log(gf)$" sequence. However, the log(*gf*) in a few dozen of the LOIs did not settle down even after 30 iterations. Instead, the parameters oscillated around certain values. This usually happened to overlapping lines with similar depth. We identified these lines in the last iterations in the "$2 \times E\log(gf)$, $2 \times E\mathrm{damp}$, $4 \times E\log(gf)$" sequence and replaced these log(*gf*) values with their average values. Figure 2 shows a "hair-diagram" for a small piece of spectrum with an illustration of log(*gf*)-stable and unstable lines. Each curve starts at its central wavelength at the *x*-axis. The *x*-deviation from the vertical designates the difference of log(*gf*) from the original value. The vertical direction shows the iterative sequence progress ($2 \times E\log(gf)$, $2 \times E\mathrm{damp}$, and then $n \times E\log(gf)$).

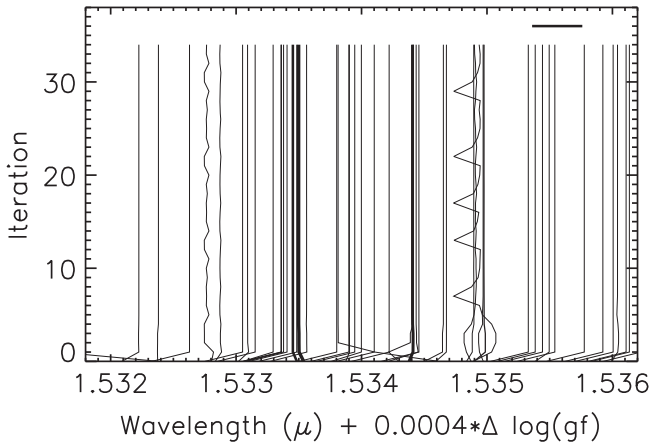


**Figure 2.** Example of log(*gf*) stability during fits to the Sun and Arcturus. The *X*-axis for this diagram is in microns combined with a scaling of offsets in log(*gf*). The horizontal bar at the top right corner corresponds to the length of a 1.0 dex change in log(*gf*). Change of the log(*gf*) with respect to the original value is shown as the deviation from the vertical line. The *Y*-axis shows the progress of the iterations: $2 \times E\log(gf)$, then $2 \times E\mathrm{damp}$, and then $n \times E\log(gf)$. Parameters of most of the lines settle down after the 3rd log(*gf*)-iteration. The line thickness denote the line depth with the thinest lines having depths less than 0.01 and the thickest lines having depths greater than 0.2.

The version of MOOG we employed to generate the astrophysical line parameters does not have a proper treatment for the damping of hydrogen lines. Thus these features were artificially removed from the atlases by dividing by a synthetic spectrum containing only hydrogen lines, where these broad features were forced to fit. The hydrogen lines were also removed from the input line list when importing it into MOOG; the final adopted line list used by APOGEE included the hydrogen lines. Molecular lines could be adjusted in a way similar to that adopted for the lines with HFS, where lines from the same multiplet or all multiplets could be adjusted by the same amount. We tried fitting the extremely weak CO, CN, and OH features in the Sun by eye for DR10. Given the weakness of the lines in the Sun, no attempt to modify the literature molecular log(*gf*) values were made for INT and DR12, so the final adopted line list is a result of an evaluation of only the atomic lines, excluding hydrogen. Figure 3 shows an example of the fitted solar spectrum. The rms scatter in the difference spectra (lower panel) is reduced from 0.021 with the base line list to 0.007 with the final DR12 line list. This improvement is seen across the spectrum and is a strong indication that this methodology works. The most important test for any line list is to verify that it produces reliable abundances results requiring no or little zero point corrections when compared with well established abundance trends and values from the literature. We refer to Holtzman et al. (2015) for such a discussion.

### 3.2. *Astrophysical log*(gf) *Values*

As described above, the astrophysical log(*gf*) values were calculated from lab log(*gf*) values (when available), taking into consideration the errors in those measurements. For DR10 and INT the astrophysical log(*gf*) values were allowed to vary within one sigma of the laboratory errors, while for DR12 this was expanded to two sigma. Figure 4 shows the difference

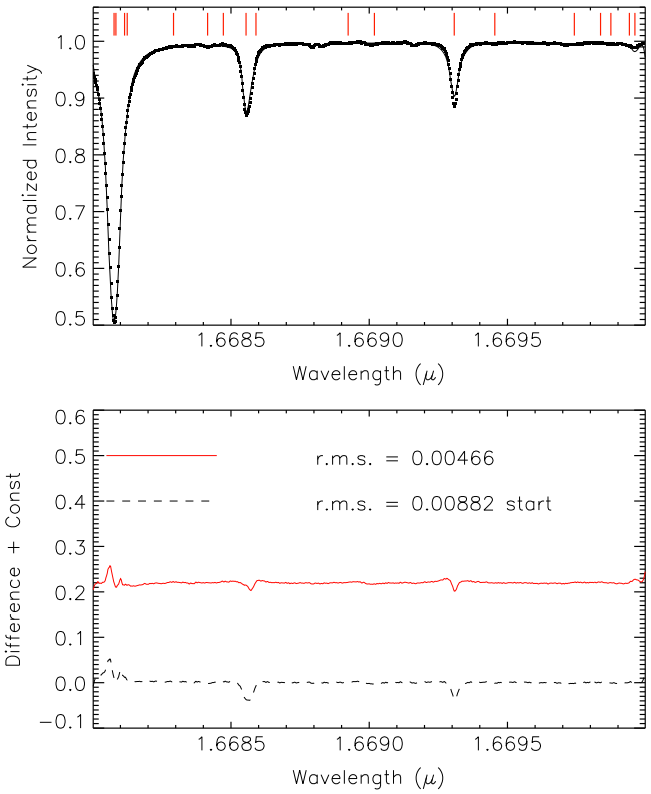


**Figure 3.** Example of the input and output spectra from the astrophysical adjustment of the line parameters. Top panel: observed solar spectrum (dots) and best-fit synthesized spectrum (solid curve). The vertical red bars designate wavelengths of lines whose parameters were adjusted. Some visible features are not fit because they are molecular features, and for the INT and DR12 line lists we made no astrophysical corrections to molecules. Bottom panel: difference between the observed and synthetic solar spectra before (lower curve) and after (upper curve) the iterations. The upper curve has been shifted by +0.2 along the vertical axis. The weakest features visible in the observed spectrum have depth of 0.004 from the continuum and equivalent widths of <0.6 mÅ, at the resolution and SNR of APOGEE spectra these features would not be visible.

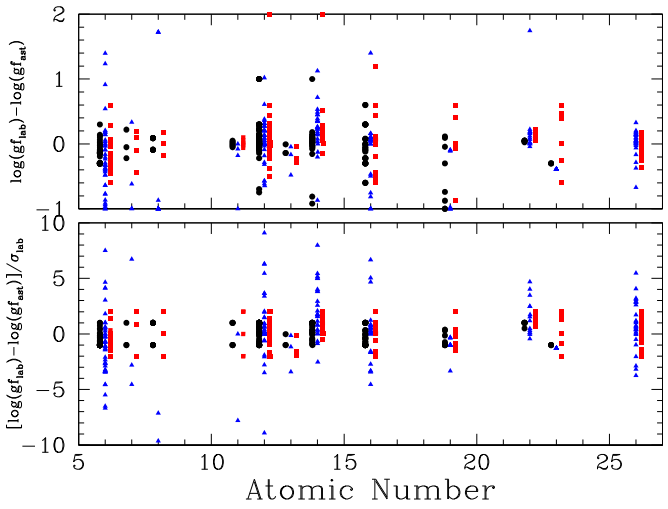


**Figure 4.** Comparison of the astrophysical and laboratory log(*gf*) values from DR10 and DR12. The top panel shows the differences between the log(*gf*) values for each line and the bottom panel shows the difference between the log(*gf*) values compared to the laboratory error in the log(*gf*) value. In this figure the black circles represent the atomic lines with lab data from DR10 and have been offset by −0.2 in atomic number for better visibility, the red squares represent the lines with lab data from DR12 and have been offset by +0.2 in atomic number for better visibility, and the blue triangles were calculated without any lab constraints using both Arcturus and the Sun with limits of −2 and +0.75 dex in log(*gf*).

between the astrophysical and laboratory log(*gf*) values (top panel) and this same difference divided by the laboratory error (bottom panel). For reference, the blue triangles in this figure show how much the log(*gf*) values would change if we adopted the same criterium used for the literature empirical log(*gf*) values, i.e., allowed changes of −2 to +0.75 dex. While some of the red squares and black circles in the lower panel of Figure 4 do fall at the one and two sigma limits, most are within the error limits and centered around zero, which lends confidence that these astrophysical log(*gf*) values are of good accuracy. The exception may be Ti, where the laboratory log(*gf*) values tend to be larger than the astrophysical log(*gf*) values in both DR10 and DR12. This may be caused by the temperature sensitivity of the Ti I lines and thus were driven by the assumed abundance of Ti in Arcturus (the cooler of the two stars constraining the astrophysical log(*gf*) values). The actual errors on the laboratory Ti I log(*gf*) values are very small and therefore the astrophysical log(*gf*) values were not allowed to vary substantially from the original laboratory log(*gf*) values. When the laboratory constraints were removed for Ti I (the blue triangles in the upper panel of Figure 4), the resulting log(*gf*) values were again not substantially different from the laboratory values, with the single exception of the Ti I transition at 16,413.029 Å.

### 3.2.1. Impact of using COD versus Total Flux

As mentioned earlier, due to an incorrect entry in the MOOG parameter file, which was recognized later on, the solar log(*gf*) values of the INT and DR12 line lists were calculated in total flux rather than as COD, even though the reference solar spectral atlas is COD. Figures 5 and 6 show the impact of the difference in the astrophysical log(*gf*) values calculated with the proper COD option set in MOOG's parameter file and the "normal" flux option. The top panel shows the log(*gf*) differences between COD and total flux for a fit only to the Sun, as was done for INT, and the bottom panel shows the differences for a fit using both the Sun and Arcturus, as was done for DR12. The Arcturus residuals are best fit with a constant offset of 0.019 dex in both figures. The INT residuals are best fit with a second order polynomial with respect to the excitation potential or a constant offset of 0.063 dex as a function of atomic numbers. This shows that by not using the appropriate COD flag set in MOOG's parameter file is more problematic for the INT line list than for DR12. The Sun-only fit could introduce a small temperature bias; a simple test using MOOG and these two line lists suggests a temperature offset of ∼40 K and a modest metallicity bias of ∼−0.05 dex, in the sense that the log(*gf*) values should have been larger and thus the derived abundances are too large. García Pérez et al. (2013) adopted the INT line list and thus was impacted by both of these zero points while Smith et al. (2013) and Cunha et al. (2015) are impacted by only the metallicity bias because their stellar effective temperatures and surface gravities were set with an independent methodology. The exact impact these biases have are somewhat dependent upon the lines adopted. For example, all abundances based on molecules should not be influenced because these lines were not adjusted after DR10 in

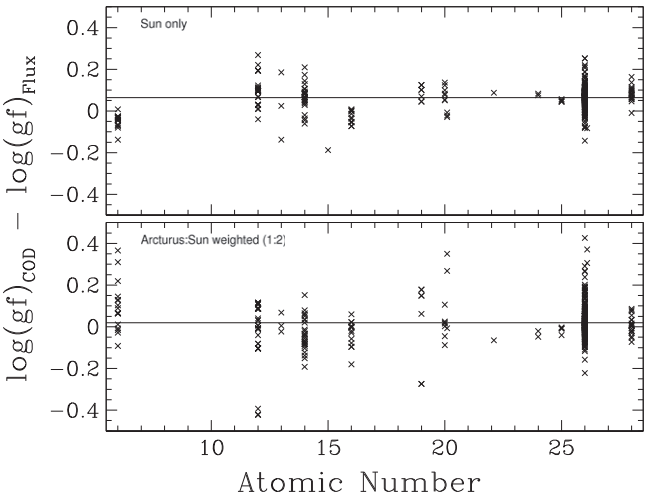


**Figure 5.** Difference between the astrophysical log(*gf*) values calculated with the proper center-of-disk (COD) option set in MOOG and the "normal" flux option set in MOOG, shown as a function of atomic number. The top panel shows the differences for a fit only to the Sun, as was done for INT, and the bottom panel shows the differences for a fit using both the Sun and Arcturus, as was done for DR12. The solid line in both panels is the best fit to the data.

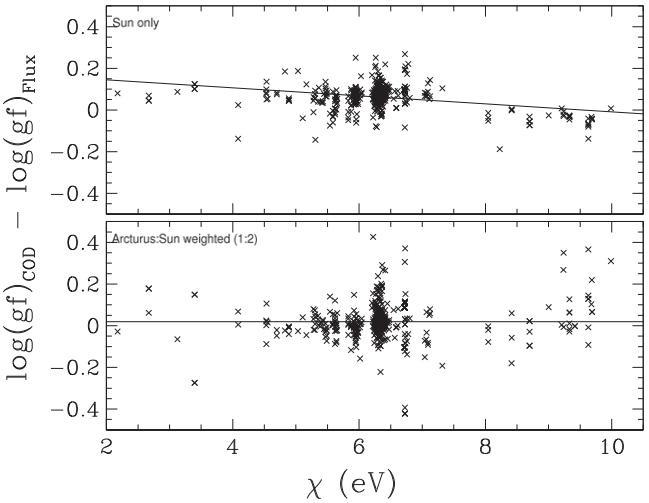


**Figure 6.** Difference between the astrophysical log(*gf*) values calculated with the proper center-of-disk (COD) option set in MOOG and the "normal" flux option set in MOOG, shown as a function of the lower level excitation potential. The top panel shows the difference for a fit only to the Sun, as was done for INT, and the bottom panel shows the differences for a fit using both the Sun and Arcturus, as was done for DR12. The solid line in both panels is the best fit to the data.

the astrophysical log(*gf*) methodology. Lines with laboratory constraints may not have been impacted depending on whether the astrophysical log(*gf*) derived was at the limits imposed by the laboratory errors.

In summary, the mean impact of this improper treatment on DR12 is less than 0.02 dex on the log(*gf*) values. In addition, there is no apparent slope with excitation potential or atomic number. Since ASPCAP determines stellar parameters using chi squared fits to the entire spectrum, the log(*gf*) values for the molecular and hydrogen lines are unchanged by the astrophysical log(*gf*) corrections, and the errors introduced by using the solar spectrum are, on average, very small, we conclude that the impact is well within the errors presented in DR12.

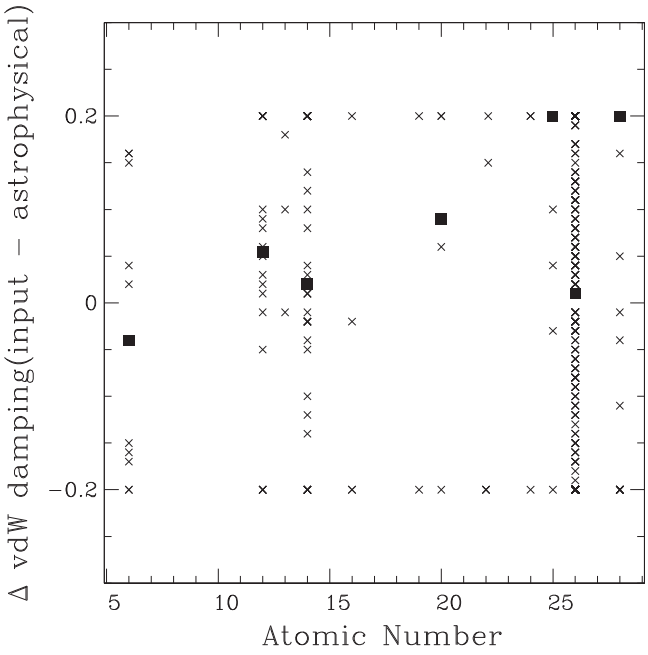


**Figure 7.** Difference between the input literature damping and the astrophysical damping values for DR12. For elements with five or more points the median value is shown as a solid square.

### 3.3. Astrophysical Damping Values

As mentioned in the previous section, after several iterations of the astrophysical log(*gf*) code we fit the line profile for the strongest lines by allowing the lines to be adjusted up to $\pm 0.2$ dex from the input damping value. Figure 7 shows the difference between the input and astrophysical damping values. The average difference for all damping values is 0.004 dex. Thus, on average, the astrophysical code is not making large changes. However, it makes a small systematic change to a few elements; for example, among Mg lines the average difference is 0.04 dex (the effect of damping is enhanced), and for the Fe lines the difference is $-0.04$ dex.

### 3.4. Performance of the Astrophysical Parameters

Over the full range of the line list the use of astrophysical log(*gf*) values improves the fit in both the Sun and Arcturus. For the DR12 line list the rms scatter of the difference between the observed spectrum and synthetic fit is 0.010 and 0.027 for the Sun and Arcturus, respectively. Without the astrophysical values the rms scatter of the differences were 0.017 and 0.032 for the Sun and Arcturus, respectively. The improvement is smaller for Arcturus since the spectrum and residuals are dominated by molecular features which are not adjusted in our astrophysical methodology for DR12. The evidence of how the line list performs is in its ability to derive quantitative abundances which can be compared to literature values for the same stars. Holtzman et al. (2015) shows that over the range: $T_{\rm eff} = 3800$–$5300$ K, $\log g = 0.5$–$3.8$ dex, $[{\rm M/H}] = -2 - +0.5$ dex, ASPCAP delivers $T_{\rm eff}$ to within 91.5 K, $\log g$ to within 0.3 dex and absolute abundances of 14 elements of 0.1–0.2 dex accuracy. This scatter is in part due to errors in the line list, but also includes errors in carbon isotope ratio mismatch, line spread function modeling errors, NLTE affects, and lack of spherical model atmospheres.

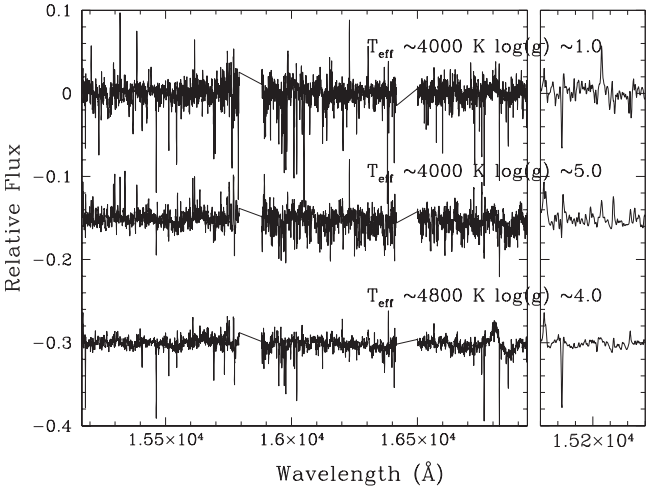


**Figure 8.** Average residual spectra (observed spectra—best fit synthetic spectra) for stars near $T_{\rm eff} \sim 4000$ K and $\log(g) \sim 1.0$ cgs dex (top), $T_{\rm eff} \sim 4000$ K and $\log g \sim 5.0$ cgs dex (middle), and $T_{\rm eff} \sim 4800$ K and $\log g \sim 4.0$ cgs dex (bottom). The left pane shows the entire APOGEE region; the breaks in the spectrum are the locations of the gaps between the detectors. The right pane contains a small region of these average residual spectra.

## 4. MISSING LINES

The analysis of more than a hundred thousand stars in APOGEE allows us to determine where the line list is either missing features or has inaccurate $\log(gf)$ values. To construct the list of missing lines we start by using the average difference between the best fit synthetic spectra and the observed spectra shifted to the rest wavelength for stars of specific effective temperatures and gravities. We have chosen to construct three average residual spectra, the first from all giant stars with $T_{\rm eff} \sim 4000$ K and $\log g \sim 1.0$ cgs dex, the second from all dwarf stars with $T_{\rm eff} \sim 4800$ K and $\log g \sim 4.0$ cgs dex, and the last one from all dwarf stars with $T_{\rm eff} \sim 4000$ K and $\log g \sim 5.0$ cgs dex. These three residual spectra are shown in Figure 8. The left pane shows the entire spectra including the gaps between the APOGEE detectors and the right pane shows a small portion of these spectra where a few strong features and several weaker features can be seen in more detail. We tabulated all residual features with depth greater than 1% (Table 6). For completeness we also included the unidentified features in the Be stars observed by APOGEE as telluric calibrators noted by Chojnowski et al. (2014). We supplemented this list with the strong lines that were not properly modeled in the analysis of a set of Fourier Transform Spectrograph (FTS) spectra of standard stars in Smith et al. (2013). Some of these lines fall between the detectors of the APOGEE instrument. For the coolest dwarfs we suspect that some of the residual features may be $H_2O$ and FeH, since those lines are known to be detected in M dwarfs in the *H* band. As mentioned in Section 2.1.1.7, we were unable to find an FeH line list that produced significant improvements for the few M dwarfs we tested. Future work on dwarfs includes MARCS/Turbospectrum modeling on these stars by including $H_2O$ and FeH (Zamora et al. 2015).

In principle, shifting the spectra to their rest wavelengths and averaging in that frame should have eliminated residual features such as badly removed telluric emission and absorption features, as well as any interstellar features. However, due to the complicated selection biases in APOGEE targeting, it is possible that some interstellar or telluric features populate Table 6. One example is the feature at 15,272.4 Å which is the strongest diffuse interstellar band (DIB) in the *H* band and is detected in the majority of APOGEE spectra (Zasowski et al. 2015). We hope that future versions of the APOGEE line list will include identifications of these types of features.

**Table 6**
Missing Lines

| λ (vac Å) | EW (mÅ) | Notes |
|---|---|---|
| 15174.1 | 18 | a |
| 15177.5 | 12 | h |
| 15178.6 | 25 | a |
| 15180.4 | 20 | a |
| 15182.3 | 61 | a, b, h |
| 15187.3 | 19 | a |
| 15201.1 | 16 | a |
| 15202.4 | 24 | a, b, h |
| 15209.7 | 39 | a |
| 15210.5 | 17 | h |
| 15211.0 | 33 | b |
| 15212.5 | 48 | a |
| 15214.5 | 16 | a |
| 15216.3 | 20 | a, b |
| 15219.4 | 59 | b |
| 15227.6 | 10 | h |
| 15228.7 | 12 | h |

**Notes.**
[a] Seen in the cool APOGEE giant spectra residual.
[b] Seen in the hot APOGEE spectra residual.
[c] Between APOGEE detectors.
[d] All FTS stars.
[e] Only M FTS stars.
[f] Found only in HD199799.
[g] See S. Hasselquist et al. 2016, in preparation.
[h] Seen in cool APOGEE dwarf spectra residuals.
[i] Seen in APOGEE Be spectra, see Chojnowski et al. (2014).
[j] This may be a DIB feature, see Zasowski et al. (2015).
[k] This may be a DIB feature, see Geballe et al. (2011).

(This table is available in its entirety in machine-readable form.)

## 5. SUMMARY

The machine readable tables and data files contain the DR10, INT and DR12 line lists in the ASPCAP format, see Tables 7 - 9. Additional copies formatted for MOOG (Sneden 1974), Synspec (Hubeny 2006; Hubeny & Lanz 2011) and Turbospectrum (Alvarez & Plez 1998; Plez 2012) are available in the electronic edition for download. The ASPCAP formatted line lists contain the baseline line list, as well as the astrophysical $\log(gf)$ and damping values. This line list is formatted in a way similar to that employed by Kurucz in his online database and CDROM releases, where wavelengths are given vacuum and in nm. Note that over the wide range of this line list, the choice of what methodology to use to translate from air to vacuum can have a significant impact. We have adopted the conversions of Ciddor (1996). See Appendix for further discussion on this choice and coefficients for conversion. For the upper and lower energy levels we use the unit $cm^{-1}$.

Some attention has been paid to HFS within these line lists but in the very strongest lines of Al the lack of the HFS components means that the abundances derived are likely to be over-estimated. Users of this line list and the abundances

**Table 7**
ASPCAP Line List Format for DR12 (20131216)

| Bytes | Format | Label | Description |
|---|---|---|---|
| 1–9 | F9.4 | lam | wavelength in vacuum nm |
| 11–17 | F7.3 | orggf | original log(*gf*) value |
| 19–25 | F7.3 | newgf | improved literature or laboratory log(*gf*) |
| 27–30 | F4.2 | enewgf | error on log(*gf*), when available |
| 32–34 | A3 | snewgf | source for improved literature or laboratory log(*gf*) |
| 35–41 | F7.3 | astgf | astrophysical log(*gf*) |
| 43–45 | A3 | sastgf | source for astrophysical log(*gf*) |
| 47–54 | F8.2 | specid | species id |
| 55–66 | F12.3 | EP1 | lower Energy Level in $cm^{-1}$ |
| 67–71 | F5.1 | J1 | *J* value for EP1 |
| 72–82 | A11 | EP1id | EP1 level identification |
| 83–94 | F12.3 | EP2 | upper Energy Level in $cm^{-1}$ |
| 95–99 | F5.1 | J2 | *J* value for EP2 |
| 100–110 | A11 | EP2id | EP2 level identification |
| 111–116 | F6.2 | Rad | Damping Rad |
| 117–122 | F6.2 | Sta | Damping Stark |
| 123–128 | F6.2 | vdW | Damping vdW |
| 130–131 | I2 | unlte | NLTE level number upper |
| 132–133 | I2 | lnlte | NLTE level number lower |
| 134–136 | I3 | iso1 | isotope number |
| 137–142 | F6.3 | hyp | hyperfine component log fractional strength |
| 143–145 | I3 | iso2 | isotope number |
| 146–151 | F6.3 | isof | log isotopic abundance fraction |
| 152–156 | I5 | hE1 | hyperfine shift for first level to be added to E1 in mK |
| 157–161 | I5 | hE2 | hyperfine shift for first level to be added to E2 in mK |
| 162 | A1 | F0 | hyperfine F symbol |
| 163 | I1 | F1 | hyperfine F for the first level |
| 164 | A1 | note1 | note on character of hyperfine data for first level: *z* none, ? guessed |
| 165 | A1 | S | the symbol "−" for legibility |
| 166 | I1 | F2 | hyperfine F' for the second level |
| 167 | A1 | note2 | note on character of hyperfine data for second level: *z* none, ? guessed |
| 168–172 | I5 | g1 | lande *g* for first level times 1000 |
| 173–177 | I5 | g2 | lande *g* for second level times 1000 |
| 178–180 | A3 | vdWorg | source for the original vdW damping |
| 181–186 | F6.2 | vdWast | astrophysical vdW damping |

**Notes.**
In addition the same DR data is available in MOOG, Turbospectrum, and AASeT formats in the included .tar.gz package.

(This table is available in its entirety in machine-readable form.)

**Table 8**
ASPCAP Line List Format for INT (20120216)

| Bytes | Format | Label | Description |
|---|---|---|---|
| Same Format as Table 7 | | | |

**Notes.**
In addition the same INT data is available in MOOG, Turbospectrum, and AASeT formats in the included .tar.gz package.

(This table is available in its entirety in machine-readable form.)

**Table 9**
ASPCAP Line List Format for DR10 (20110510)

| Bytes | Format | Label | Description |
|---|---|---|---|
| Same Format as Table 7 | | | |

**Notes.**
In addition the same DR data is available in MOOG, Turbospectrum, and AASeT formats in the included .tar.gz package.

(This table is available in its entirety in machine-readable form.)

of Al should be wary in the strongest lined and coolest stars.

This line list has been tuned to be applied to red giants over a range that covers F, G, K and warm M giants. Tests conducted by the APOGEE team suggest that it also performs adequately for F, G, and K dwarfs. These line lists does not contain the FeH lines nor the $H_2O$ lines needed to model cool M giants or M dwarfs. The reader is cautioned when using these line lists outside these stellar types or on stars with extreme abundance patterns such as carbon stars where other molecular features may play an important role and these line lists have not been tested. In addition, the use of the astrophysical log(*gf*) values derived for this work should be approached with caution when using a different spectral synthesis code or suite of model atmospheres. See Sections 3 and 4 of Zamora et al. (2015) for more extensive information about the tests that have been conducted and possible systematics that could be introduced.

The ASPCAP machine readable line lists (Tables 7–9) are ∼24 MB in size with 35 columns and ∼134,000 rows of data.

For a detailed discussion on how these line lists performed we point the reader to Mészáros et al. (2013) and Lamb et al. (2015) for DR10 performance, Smith et al. (2013) for discussions of the INT line list, and Mészáros et al. (2015) and Holtzman et al. (2015) for DR12 performance. Mészáros et al. (2013) compared literature metallicity, effective temperature, and surface gravity to the values computed by ASPCAP for DR10. They found some systematic offsets in gravity and metallicity. The source of these offsets may not be the line list but rather the methodology within the DR10 version of ASPCAP. Lamb et al. (2015) conducted an independent manual analysis of several metal-poor globular clusters stars with optical spectra and APOGEE DR10 spectra and line list. They found good agreement for Fe, Mg, and Ca lines, but had a concern about the single detectable Ti I line (15,339 Å vac) being a blend. Lamb et al. (2015) adopted an average between the optical and *H*-band results for Fe, Mg, and Ca and adopted the *H*-band results for Al, Si, O, C, and N. Smith et al. (2013) conducted an independent manual analysis of several very high-resolution, very high S/N FTS spectra using the INT line list. In a comparison of their results to the literature, they found agreement within ∼0.1 dex for all abundances they derived: $^{12}C$, $^{13}C$, N, O, Mg, Al, Si, K, Ca, Ti, V, Cr, Mn, Fe, Co, Ni, and Cu. Cunha et al. (2015) analyzed manually, also using the INT line list, a sample of red giants and clump stars in the very metal rich open cluster NGC6791 and found overall good agreement with optical results from the literature for the abundances of oxygen, sodium and iron.

Mészáros et al. (2015) derived abundances in an independent manual analysis of APOGEE spectra of 10 globular clusters using the DR12 line list. They derived abundances for nine elements and found good agreement for most elements, once zero point differences in adopted solar abundances are considered. Exceptions included Ti and Ca, which exhibited

a large scatter in the APOGEE results, and Al, which are based on very weak spectral lines in the literature optical analyses and on very strong features in the *H* band. Holtzman et al. (2015) analyzed the ASPCAP DR12 results for self consistency within clusters and also did comparisons with abundance results in the literature. They found that DR12 results had an internal abundance consistency at the level of 0.05–0.09 dex and 0.1–0.2 dex agreement with literature values. This study, however, pointed out a number of elements which exhibited unexpected trends with respect to metallicity. In particular, for the entire APOGEE sample, the mean abundances of S, Si, and Ca at roughly solar metallicities were above the solar value, and Ti does not exhibit the expected rise at decreasing metallicity seen in the literature. These types of analyses and, in particular, comparisons with cluster abundance results can act as a guide for future improvements to the line list.

Funding for SDSS-III has been provided by the Alfred P. Sloan Foundation, the Participating Institutions, the National Science Foundation, and the U.S. Department of Energy Office of Science. The SDSS-III web site is http://www.sdss3.org/.

SDSS-III is managed by the Astrophysical Research Consortium for the Participating Institutions of the SDSS-III Collaboration including the University of Arizona, the Brazilian Participation Group, Brookhaven National Laboratory, Carnegie Mellon University, University of Florida, the French Participation Group, the German Participation Group, Harvard University, the Instituto de Astrofisica de Canarias, the Michigan State/Notre Dame/JINA Participation Group, Johns Hopkins University, Lawrence Berkeley National Laboratory, Max Planck Institute for Astrophysics, Max Planck Institute for Extraterrestrial Physics, New Mexico State University, New York University, Ohio State University, Pennsylvania State University, University of Portsmouth, Princeton University, the Spanish Participation Group, University of Tokyo, University of Utah, Vanderbilt University, University of Virginia, University of Washington, and Yale University.

S.M. has been supported by the János Bolyai Research Scholarship of the Hungarian Academy of Sciences. D.A.G.H. and O.Z. acknowledge support provided by the Spanish Ministry of Economy and Competitiveness under grants AYA-2011-27754 and AYA-2014-58082-P. D.B. was supported by grant RSF 14-50-00043. We would like to thank R.L. Kurucz for his many fundamental contributions that have made this work possible.

## APPENDIX
## AIR-VACUUM CONVERSION

Since the APOGEE spectrograph is operating in vacuum, it was natural for APOGEE to adopt a vacuum wavelength scale. Further support for embracing a vacuum scale is motivated by the fact that, historically, the definition of standard air includes tight constrains on temperature (15 C), pressure (1 atmosphere), and humidity (dry), but not so clearly the CO2 concentration, which is time and spatially dependent, and the standard temperature scale has also seen multiple changes in the past century, and these drag the air-to-vacuum corrections. In addition, the reference wavelengths for the Th and Ar lines usually employed for calibration come from vacuum-housed spectrographs, and are therefore more naturally used in vacuum (Norlén 1973; Palmer & Engleman 1983; Hinkle et al. 2001; Lovis & Pepe 2007; Kerber et al. 2008). This Appendix describes the differences on the vacuum-to-air conversions and motivates APOGEE adopting a specific one for dealing with such corrections.

### *A.1. Available Formulae*

The IAU standard for the vacuum to standard air corrections (see resolution No. C15, Commission 44, XXI General Assembly in 1991) refers to Oosterhoff (1957), which adopts the results by Edlén (1953).

$$\frac{\lambda_0 - \lambda}{\lambda} = n - 1 = a + \frac{b1}{c1 - 1/\lambda_0^2} + \frac{b2}{c2 - 1/\lambda_0^2} \quad (1)$$

where $\lambda_0$ is given in $\mu$m, and the constants are given in the first row of Table 10. Later work widely adopted in the physics literature by Edlén (1966) rederived the constants from optical and near UV data, and later Peck & Reeder (1972, and references therein) added additional measurements extending into the IR, up to 1.7 $\mu$m, which showed a systematic deviation from Edléns equation at the level of several $10^{-9}$, or a few $ms^{-1}$.

Table 10 compares the parameters proposed by Edlén (1953, 1966), Peck & Reeder (1972), and Ciddor (1996), the latter reference largely based on Peck & Reeder (1972), but updated to account for the changes taken place in the international temperature scale since their work, and adjusting the results for the $CO_2$ concentration. Figure 9 shows a maximum discrepancies at the level of $3 \times 10^{-8}$, or 10 $ms^{-1}$ at 1.6 $\mu$m. The equations proposed by Edlén (1966) and Peck & Reeder (1972) differ only by about one fourth of that. About half of the difference between Peck & Reeder and Ciddor ($2 \times 10^{-8}$ or 6.5 $ms^{-1}$ at 1.6 $\mu$m) is related to the temperature scale. The paper by Peck & Reeder is not specific regarding the scale used, and Ciddor assumes they used the IPTS-48 standard[16], which is warmer than the one currently in use (ITS-90) by 9.2 mK at 15 C. If Peck & Reeder used the IPTS-68 standard instead, the difference would be reduced to 5.6 mK. Changes of 9.2 mK and 5.6 mK amount to an increase in $(n - 1) \times c$ of about 2.6 and 1.6 $m^{-1}$, respectively, at 1.6 $\mu$m. The rest of the correction between Peck & Reeder and Ciddors review (3.9 $ms^{-1}$ at 1.6 $\mu$m) is related to the $CO_2$ concentration in standard air. Because of secular variations in the typical laboratory air, Birch & Downs proposed to use 450 ppm in the definition of standard air, while Ciddor estimates that a value closer to 300 ppm is adequate for the measurements used by Peck & Reeder. In summary, the variation between between Peck & Reeder (1972) and Ciddor (1996) is connected to a change between the actual conditions of standard air now and at the time of the measurements.

### *A.2. Conclusions*

In view of the preceding discussion, we underline the advantages of using vacuum wavelengths for the APOGEE spectra. In some cases, corrections between air and vacuum will be needed, and for those it is proposed that the formulation proposed by Ciddor (1996) be used. This corresponds to Equation (1) with the Ciddor constants given in Table 10. This

[16] International Practical Temperature Scale; $t_{68} = 1.00024 \times t_{90}$ (Saunders 1990); $t_{68} = t_{48} - 4.4 \times 10^{-6} t_{48} \times (100 - t_{48})$ (Fofonoff & Bryden 1975).

**Table 10**
Parameters for Equation (1)

| References | $a$ | $b1$ | $b2$ | $c1$ | $c2$ |
|---|---|---|---|---|---|
| Edlén (1953) | $6.4328 \times 10^{-5}$ | $2.94981 \times 10^{-2}$ | $2.5540 \times 10^{-4}$ | 146.0 | 41.0 |
| Edlén (1966) | $6.4328 \times 10^{-5}$ | $2.406030 \times 10^{-2}$ | $1.5997 \times 10^{-4}$ | 130.0 | 38.9 |
| Peck & Reeder (1972) | 0.0 | $5.791817 \times 10^{-2}$ | $1.67909 \times 10^{-3}$ | 238.0185 | 57.362 |
| Ciddor (1996) | 0.0 | $5.792105 \times 10^{-2}$ | $1.67917 \times 10^{-3}$ | 238.0185 | 57.362 |

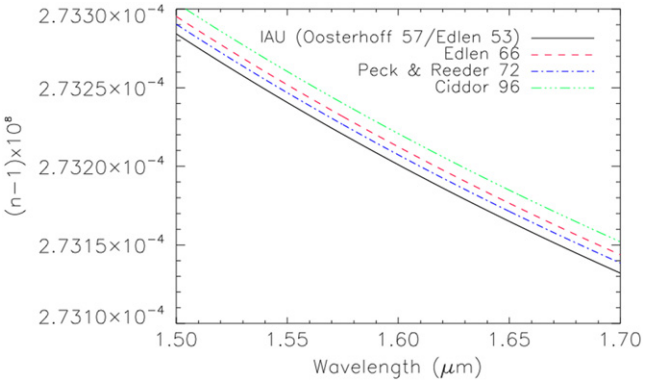


**Figure 9.** Difference between the refractive index of standard air ($n$) and unity in the $H$ band for four different sources considered.

is valid for the wavelength range between 0.23 and 1.7 $\mu$m, and the estimated accuracy in the predicted refraction index of standard air is about $10^{-8}$ or roughly 3 ms$^{-1}$ at 1.6 $\mu$m. Note that it is straightforward to go from vacuum to standard air wavelengths with Equation (1), but the inverse process requires iteration since n is given as a function of vacuum wavelength.

## REFERENCES


Abia, C., Palmerini, S., Busso, M., & Cristallo, S. 2012, A&A, 548, A55
Ahn, C. P., Alexandroff, R., Allende Prieto, C., et al. 2014, ApJS, 211, 17
Alam, S., Albareti, F. D., Allende Prieto, C., et al. 2015, ApJS, 219, 12
Alvarez, R., & Plez, B. 1998, A&A, 330, 1109
Asplund, M., Grevesse, N., & Sauval, A. J. 2005, in ASP Conf. Series, Vol. 336, Cosmic Abundances as Records of Stellar Evolution and Nucleosynthesis, ed. T. G. Barnes, III & F. N. Bash (San Francisco, CA: ASP), 25
Asplund, M., Grevesse, N., Sauval, A. J., & Scott, P. 2009, ARA&A, 47, 481
Barklem, P. S., Anstee, S. D., & O'Mara, B. J. 1998, PASA, 15, 336
Bender, C., Simon, M., Prato, L., Mazeh, T., & Zucker, S. 2005, AJ, 129, 402
Biémont, E., Palmeri, P., & Quinet, P. 1999, Ap&SS, 269, 635
Bizyaev, D., & Shetrone, M. 2015, Astrophysics Source Code Library, ascl:1502.022
Blackwell-Whitehead, R. J., Lundberg, H., Nave, G., et al. 2006, MNRAS, 373, 1603
Brault, J. W., Testerman, L., Grevesse, N., et al. 1982, A&A, 108, 201
Castelli, F., Gratton, R. G., & Kurucz, R. L. 1997, A&A, 318, 841
Chojnowski, S. D., Whelan, D. G., Wisniewski, J. P., et al. 2014, arXiv:1409.4668
Ciddor, P. E. 1996, ApOpt, 35, 1566
Claret, A. 2000, A&A, 363, 1081
Cunha, K., Smith, V. V., Johnson, J. A., et al. 2015, ApJL, 798, L41
Dulick, M., Bauschlicher, C. W., Jr., Burrows, A., et al. 2003, ApJ, 594, 651
Edlén, B. 1953, JOSA, 43, 339
Edlén, B. 1966, Metro, 2, 71
Eisenstein, D. J., Weinberg, D. H., Agol, E., et al. 2011, AJ, 142, 72
Falkenburg, & Zimmermann 1979, Naturforsch, 34a, 1249
Fofonoff, N. P., & Bryden, H. 1975, JMR, 33, 69
García Pérez, A. E., Cunha, K., Shetrone, M., et al. 2013, ApJ, 767, 9
García Pérez, A. E., Allende Prieto, C., Holtzman, J. A., et al. 2015, arXiv:1510.07635
Geballe, T. R., Najarro, F., Figer, D. F., Schlegelmilch, B. W., & de La Fuente, D. 2011, Natur, 479, 200
Goldman, A., Shoenfeld, W. G., Goorvitch, D., et al. 1998, JQSRT, 59, 453
Goorvitch, D. 1994, ApJS, 95, 535
Gray, D. F. 1981, ApJ, 245, 992
Gray, D. F., & Brown, K. I. 2006, PASP, 118, 1112
Grevesse, N., Noels, A., & Sauval, A. J. 1996, in Cosmic Abundances, Vol. 99, ed. S. S. Holt & G. Sonneborn (San Francisco, CA: ASP), 117
Gunn, J. E., Siegmund, W. A., Mannery, E. J., et al. 2006, AJ, 131, 2332
Gustafsson, B., Edvardsson, B., Eriksson, K., et al. 2003, in Stellar Atmosphere Modeling, Vol. 288, ed. I. Hubeny, et al. (San Francisco, CA: ASP), 331
Gustafsson, B., Edvardsson, B., Eriksson, K., et al. 2008, A&A, 486, 951
Güzelçimen, F., Basar, G., Öztürk, I. K., et al. 2011, JPhB, 44, 215001
Güzelçimen, F., Yapıcı, B., Demir, G., et al. 2014, ApJS, 214, 9
Hansen, Laughlin, van der Hart, & Verbockhaven 1999, JPhB, 32, 2099
Happer, W. 1974, in Atomic Physics, Vol. 4, ed. G. zu Putlitz, E. W. Weber, & A. Winnacker (New York: Plenum)
Hinkle, K., Wallace, L., & Livingston, W. D. 1995, PASP, 107, 1042
Hinkle, K. H., Joyce, R. R., Hedden, A., Wallace, L., & Engleman, R., Jr. 2001, PASP, 113, 548
Holtzman, J. A., Shetrone, M., Johnson, J. A., et al. 2015, arXiv:1501.04110
Hubeny, I. 2006, in Computational Methods in Transport, ed. F. Graziani (Berlin: Springer)
Hubeny, I., & Lanz, T. 2011, Astrophysics Source Code Library, ascl:1109.022
Kelleher, D. E., & Podobedova, L. I. 2008, JPCRD, 37, 267
Kerber, F., Nave, G., & Sansonetti, C. J. 2008, ApJS, 178, 374
Koesterke, L. 2009, in AIP Conf. Series, Vol. 1171, RECENT DIRECTIONS IN ASTROPHYSICAL QUANTITATIVE SPECTROSCOPY AND RADIATION HYDRODYNAMICS: Proceedings of the International Conference in Honor of Dimitri Mihalas for His Lifetime Scientific Contributions on the Occasion of His 70th Birthday, ed. I. Hubeny et al. (New York: AIP), 73
Kokkin, D. L., Bacskay, G. B., & Schmidt, T. W. 2007, JChPh, 126, 084302
Kramida, A., Ralchenko, Y., Reader, J. & NIST ASD Team 2014, NIST Atomic Spectra Database (ver. 5.2), [Online]. Available: http://physics.nist.gov/asd [2014, October 17]. National Institute of Standards and Technology, Gaithersburg, MD
Lamb, M., Venn, K., Shetrone, M., Sakari, C., & Pritzl, B. 2015, MNRAS, 448, 42L
Langhoff, S. R., & Bauschlicher, C. W. 1990, JMoSp, 141, 243
Laughlin, C. 1992, PhyS, 45, 238
Lawler, J. E., Guzman, A., Wood, M. P., Sneden, C., & Cowan, J. J. 2013, ApJS, 205, 11
Livingston, W., & Wallace, L. 1991, in NSO Technical Report, An Atlas of the Solar Spectrum in the Infrared from 1850 to 9000 cm$^{-1}$ (1.1 to 5.4 microns) (Tucson, AZ: National Solar Observatory), #91-001
Lovis, C., & Pepe, F. 2007, A&A, 468, 1115
Majewski, S. R., Schiavon, P., Frinchaboy, P. M., et al. 2015, arXiv:1509.05420
Martin, G. A., Fuhr, J. R., & Wiese, W. L. 1988, JPCRD, 17, 512
McWilliam, A., Preston, G. W., Sneden, C., & Searle, L. 1995, AJ, 109, 2757
Melendez, J., & Barbuy, B. 1999, ApJS, 124, 527
Mészáros, S., Allende Prieto, C., Edvardsson, B., et al. 2012, AJ, 144, 120
Mészáros, S., Holtzman, J., García Pérez, A. E., et al. 2013, AJ, 146, 133
Mészáros, S., Martell, S. L., Shetrone, M., et al. 2015, AJ, 149, 153
Nelder, J. A., & Mead, R. 1965, CompJ, 7, 308
Nidever, D. L., Holtzman, J. A., Allende Prieto, C., et al. 2015, arXiv:1501.03742
Norlén, G. 1973, PhyS, 8, 24
Oosterhoff, P. T. 1957, Trans. IAU, 9, 69
Palmer, B. A., & Engleman, R. 1983, Los Alamos National Laboratory Report, LA-9615 (LA, Los Alamos: National Laboratory)
Palmeri, P., Biemont, E., Aboussaid, A., & Godefroid, M. 1995, JPhB, 28, 3741
Palmeri, P., Biemont, E., Quinet, P., et al. 1997, PhyS, 55, 586

Peck, E. R., & Reeder, K. 1972, JOSA, 62, 958
Plez, B. 2012, Astrophysics Source Code Library, ascl:1205.004
Podobedova, L. I., Kelleher, D. E., & Wiese, W. L. 2009, JPCRD, 38, 171
Prato, L., Simon, M., Mazeh, T., et al. 2002, ApJ, 569, 863
Ruffoni, M. P., Allende Prieto, C., Nave, G., & Pickering, J. C. 2013, ApJ, 779, 17
Ryde, N., Edvardsson, B., Gustafsson, B., et al. 2009, A&A, 496, 701
Ryde, N., Gustafsson, B., Edvardsson, B., et al. 2010, A&A, 509, A20
Safronova, M. S., Johnson, W. R., & Derevianko, A. 1999, PhRvA, 60, 4476
Saloman, E. B. 2012, JPCRD, 41, 013101
Sansonetti, J. E. 2006, JPCRD, 35, 301 Erratum 37, 1183 (2008)
Sansonetti, J. E. 2008, JPCRD, 37, 1659
Saunders, P. 1990, The International Temperature Scale of 1990, ITS-90. WOCE Newsletter 10
Smith, V. V., Cunha, K., Shetrone, M. D., et al. 2013, ApJ, 765, 16
Sneden, C. 1974, PhD Thesis, Univ. Texas at Austin
Sneden, C., Lucatello, S., Ram, R. S., Brooke, J. S. A., & Bernath, P. 2014, ApJS, 214, 26
Sur, C., Chaudhuri, R. K., Das, B. P., & Mukherjee, D. 2005, JPhB, 38, 4185
Thorne, A. P., Pickering, J. C., & Semeniuk, J. 2011, ApJS, 192, 11
Unsöld, A. 1955, Physik der Sternatmospharen MIT besonderer Berucksichtigung der Sonne (Berlin: Springer)
Wiese, W. L., & Fuhr, J. R. 2007, JPCRD, 36, 1287
Wiese, W. L., & Fuhr, J. R. 2009, JPCRD, 38, 565
Wiese, W. L., Fuhr, J. R., & Deters, T. M. 1996, (Melville, NY: AIP Press)
Wiese, W. L., Smith, M. W., & Miles, B. M. 1969, Nat. Stand. Ref. Data Ser., NSRDS-NBS 22 (Washington, DC: U.S. Government Printing Office), 268
Wood, M. P., Lawler, J. E., Sneden, C., & Cowan, J. J. 2013, ApJS, 208, 27
Wood, M. P., Lawler, J. E., den Hartog, E. A., Sneden, C., & Cowan, J. J. 2014, ApJS, 214, 18
Wyart, J.-F., & Palmeri, P. 1998, PhyS, 58, 368
Zamora, O., García-Hernández, D. A., Allende Prieto, C., et al. 2015, AJ, 149, 181
Zasowski, G., Johnson, J. A., Frinchaboy, P. M., et al. 2013, AJ, 146, 81
Zasowski, G., Ménard, B., Bizyaev, D., et al. 2015, ApJ, 798, 35